

---

# Guided Latent Slot Diffusion for Object-Centric Learning

---

Krishnakant Singh<sup>†,1</sup> Simone Schaub-Meyer<sup>1,2</sup> Stefan Roth<sup>1,2</sup>

<sup>1</sup>Dept. of Computer Science, TU Darmstadt <sup>2</sup>hessian.AI

## Abstract

Slot attention aims to decompose an input image into a set of meaningful object files (slots). These latent object representations enable various downstream tasks. Yet, these slots often bind to object parts, not objects themselves, especially for real-world datasets. To address this, we introduce Guided Latent Slot Diffusion – GLASS, an object-centric model that uses generated captions as a guiding signal to better align slots with objects. Our key insight is to learn the slot-attention module in the space of generated images. This allows us to repurpose the pre-trained diffusion decoder model, which reconstructs the images from the slots, as a semantic mask generator based on the generated captions. GLASS learns an object-level representation suitable for multiple tasks simultaneously, *e.g.*, segmentation, image generation, and property prediction, outperforming previous methods. For object discovery, GLASS achieves approx. a +35% and +10% relative improvement for mIoU over the previous state-of-the-art (SOTA) method on the VOC and COCO datasets, respectively, and establishes a new SOTA FID score for conditional image generation amongst slot-attention-based methods. For the segmentation task, GLASS surpasses SOTA weakly-supervised and language-based segmentation models, which were specifically designed for the task.

## 1 Introduction

Humans perceive a scene as a collection of objects. Such a decomposition of the scene [34] into objects makes humans capable of higher cognitive tasks like control, reasoning, and the ability to generalize to unseen experiences [23]. Building on these ideas, object-centric learning (OCL) aims to decompose a scene into compositional and modular symbolic components. OCL methods bind these components to latent representations, enabling these models to be applied to tasks like causal inference [61], reasoning [3], control [5], and out-of-distribution generalization [14].

Slot attention-based models [45], a popular class of OCL methods, decompose an image into a set of latent representations where each element, called a slot, competes to represent a part of the image. Slot attention methods can be categorized as latent scene representation networks, where the scene representation (slots) can be used for various downstream tasks [45] such as property prediction [14], image reconstruction [31], image editing [77], and object discovery [63].

A major challenge for OCL methods has been their applicability to real-world scenes. For example, slot attention-based approaches [45, 65, 66] initially showed promising results *only* for toy or synthetic datasets like CLEVR [32, 35] and MOVi [24], which have comparatively simple textures and shapes. Recently, DINOSAUR [63] and diffusion-based slot attention methods [30, 77] showed promising results on real-world datasets such as COCO [43] and VOC [20]. In particular, StableLSD [31] showed that using a pre-trained Stable Diffusion [56] model as a decoder not only leads to better

---

<sup>†</sup>Corresponding author email: [krishnakant.singh@tu-darmstadt.de](mailto:krishnakant.singh@tu-darmstadt.de)  
Project website: <https://guided-sa.github.io>

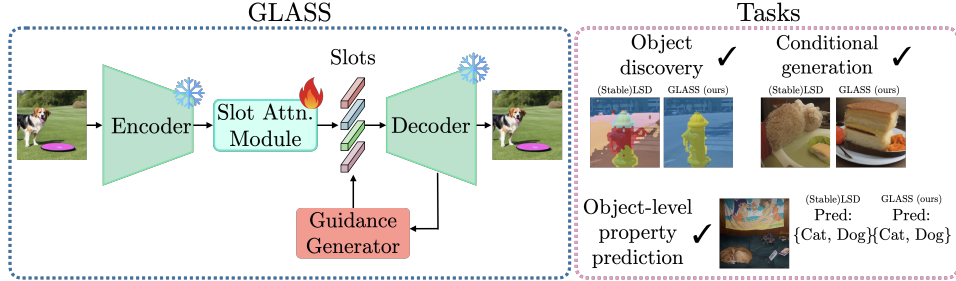


Figure 1: (left) **High-level architecture of GLASS**, based on a pre-trained diffusion model as its decoder module. GLASS learns in the space of generated images, which helps us extract the guiding signal from the decoder module for obtaining better slot embeddings. Architecture details are illustrated in Fig. 2. (right) **GLASS can perform multiple tasks** using the learned slot embeddings, such as object discovery, conditional generation, and object-level property prediction. GLASS outperforms existing OCL methods [31, 63, 77] for the object discovery and conditional generation.

object discovery for real-world datasets but can also be used for conditional reconstruction and property prediction tasks. Still, these methods lag behind weakly-supervised segmentation models [58, 59] and language-based [36, 46] segmentation methods for the task of object discovery. This performance gap can mainly be attributed to the challenges imposed by the part-whole hierarchy [28, 77]. The part-whole hierarchy can be described as the struggle to decide if an object should be segmented into its parts or as a whole object in the scene (see Fig. 1 (right), *Obj. discovery*). Our work aims to alleviate this issue and bridge the gap for object discovery while improving other tasks, such as conditional image generation and object-level property prediction.

We take inspiration from principles of Gestalt psychology [73, 74], categorizing objects based on similarity, proximity, closure, and common region to design a model that adheres to these principles to solve the part-whole hierarchy ambiguity. Instead of handcrafting such inductive biases, we posit that large generative models, such as Stable Diffusion [56], already have a notion of an object that agrees with the above principles. We propose **Guided-Latent Slot Diffusion**, GLASS, a slot attention-based method, which uses a frozen pre-trained diffusion model as its decoder and as a guidance generator (see Fig. 1 (left)). In particular, GLASS uses the pre-trained diffusion model to generate images and learns the slot attention module in the space of these generated images. This simple idea of learning in the space of generated images allows us to use the pre-trained diffusion model as a semantic mask extraction engine in addition to it being employed as the decoder. The key to our decision is based on two simple observations: (1) Learning on synthetic images generalizes well to real images [21, 60, 67, 69], and (2) learning with synthetic images allows us to use a pre-trained diffusion model such as Stable Diffusion [56] as a pseudo ground-truth generation engine. GLASS utilizes generated image captions to obtain the semantic masks from pre-trained diffusion models. These semantic masks are then used for guiding slots in the slot attention module using a *guidance loss*. This enables the slots to learn better slot embeddings, which are more object-centric. We show that GLASS segments objects better than previous SOTA OCL methods [31, 63, 77] and our guided slots are able to generate more realistic looking images compared to the previous SOTA OCL method *i.e.* StableLSD [31].

In summary, (i) we devise GLASS, a novel OCL method, which *guides* slots to objects using a novel *guidance loss*. GLASS utilizes a pre-trained diffusion model as a semantic mask generation engine in addition to being used as a decoder of the slots to an image. (ii) Our method only requires an additional BLIP-2 model compared to StableLSD, one of the SOTA models for OCL, for generating a guidance signal. BLIP-2 is trained with images and captions, which are widely available on the internet at no cost [54, 62, 64]. Thus, the performance improvement of GLASS entails only minor human effort and is essentially free. We outperform other models that use captions [46, 55, 76, 84] and even methods that use stronger supervision signals such as bounding boxes [40] or ground-truth image-level labels [2, 58] for object discovery. (iii) Our method shows large improvements (approx. +35% (VOC) and +10% (COCO) mIoU) over previous SOTA OCL [63] methods for object discovery. (iv) GLASS establishes a new SOTA FID score amongst OCL methods for conditional image generation task. (v) We show that GLASS outperforms other weakly supervised OCL methods

Table 1: **Comparison of capabilities of GLASS with prior methods for solving downstream tasks.** The rows indicate whether each method (1) has been demonstrated on real-world data, (2) can perform object discovery (segmentation) of objects, (3) is designed to provide latents for each object, which can be used for downstream tasks, (4) can reconstruct the given image from latents. (✓) denotes whether the model can perform the task well only on synthetic datasets [24, 32, 35].

	SSL and WSL models					Language-based							OCL methods				
	STEGO [25]	PiCIE [10]	IStage [2]	AFA [58]	ToCo [59]	MaskCLIP [84]	SegCLIP [46]	CLIPpy [55]	OVSeg. [80]	OVDiff [36]	DiffuMask [76]	Dataset Diff. [49]	Slot Attention [45]	DINOSAUR [63]	SlotDiffusion [77]	StableLSD [31]	GLASS (ours)
(1) Real-world data	✓	✓	✓	✓	✓	✓	✓	✓	✓	✓	✓	✓	✗	✓	✓	✓	✓
(2) Object discovery (OD)	✓	✓	✓	✓	✓	✓	✓	✓	✓	✓	✓	✓	✓	✓	✓	✓	✓
(3) Object latents for downstream tasks (PP)	✗	✗	✗	✗	✗	✗	✗	✗	✗	✗	✗	✗	(✓)	✓	✓	✓	✓
(4) Conditional generation (CG)	✗	✗	✗	✗	✗	✗	✗	✗	✗	✗	✗	✗	(✓)	✗	✗	✓	✓

that make use of extra information like bounding box information [40] or knowing the number of objects in a scene [85].

## 2 Related work

**Unsupervised and weakly-supervised object discovery.** Self-supervised models (SSL) learn a general representation for an image by solving pretext tasks like context prediction [15], image denoising [71], and many others [7, 50, 53, 82, 83]. Methods like STEGO [25] and PiCIE [10] have shown that these image representations can be used for unsupervised segmentation of the input image with large benefits. Unlike OCL-based methods, these models cannot perform object-level reasoning because they learn a single embedding for the input image or reconstruct the input from the learned image representations. Due to their unsupervised training objective, SSL models suffer from the part-whole hierarchy ambiguity, leading to poor object segmentation. Weakly-supervised models (WSL) [2, 58, 59] try to resolve the part-whole hierarchy using additional weak annotation signals such as image-level labels or saliency maps. These methods perform better than SSL methods for the segmentation task. Still, WSL segmentation methods are only designed to perform segmentation and cannot perform other tasks, like image generation or object-level reasoning.

**Language-based segmentation methods.** Several works have shown that a pre-trained CLIP [54] model can be used for the object discovery task either by modifying the architecture [13, 55] or by learning on top of CLIP features [9, 48]. Other works like GroupViT [78] show that learning an alignment between group and text tokens using contrastive learning, even without CLIP features, is enough for object discovery. Recently, [36, 37, 49, 52, 76, 79] show that object discovery is possible using just image-level labels or captions by extracting spatial information about objects in an image from the U-Net layers of a large-scale pre-trained diffusion model like Stable Diffusion [56]. Some of these methods [52, 79], in addition to language cues, even require access to ground-truth masks. Unlike OCL-based methods, language-based segmentation models are limited to segmentation tasks due to their design and cannot conditionally generate images or perform object-level reasoning.

**Object-centric learning** decomposes a multi-object scene into a set of composable and meaningful entities using an autoencoding objective [6, 12, 18, 19, 22, 23, 33, 45, 66]. OCL methods are object-level representation learning methods that can be employed for various downstream tasks, such as segmentation, conditional generation, and object-level property prediction. Among OCL methods, slot attention-based methods have proven the most effective; they employ a set bottleneck layer of limited capacity for reconstructing the input signal. A major challenge for slot attention methods has been their poor performance on real-world scenes [81]. Using large-scale pre-trained models as encoder [63] and decoder [31, 77] has proven an effective solution, leading to promising results for real-world datasets. Yet, these models still suffer from the part-whole hierarchy ambiguity, hampering the quality of the learned slot embedding. GLASS is inspired by StableLSD [31], using a pre-trained diffusion decoder as its decoder. Unlike StableLSD, GLASS learns in the space of generated images, which allows us to repurpose the decoder model as a guidance signal generator, see Fig. 1 (left), to learn better slot embeddings and improve the performance on downstream tasks.

**Weakly-supervised object-centric learning.** Several methods have tried tackling the part-whole hierarchy ambiguity plaguing OCL methods with additional weak supervision signals. For example, video-based OCL methods used motion [40, 68] and depth cues [17]. Depth and motion cues are not available or are unreliable for images, which is the main focus of this work. Position [38, 40] and shape [16] are more effective additional cues for images. Existing weakly-supervised OCL methods remain limited to synthetic datasets, while we focus on real-world datasets. Thus, we also propose two weakly-supervised versions of the StableLSD model, which utilize additional cues in the form of bounding box information (similar to [40]) and the number of objects in the scene (identical to [85]). We find GLASS to be much superior to both these weakly-supervised variants of StableLSD.

A summary of each model’s capability to perform various downstream tasks is shown in Table 1. StableLSD and GLASS are the only models that can perform all the tasks on real-world datasets.

### 3 Preliminaries

**Slot attention** [45] is an iterative refinement scheme based on a set  $\mathbf{S} \in \mathcal{R}^{O \times d_{\text{slots}}}$ , composed of  $O$  slots of dimension  $d_{\text{slots}}$ , which are initialized either randomly or via a learned function. Once initialized, the representations of the slots are updated iteratively using a GRU network [11] based on the feature matrix  $\mathbf{H} \in \mathcal{R}^{N \times d_{\text{input}}}$  of the encoded input image, containing  $N$  feature vectors of dimension  $d_{\text{input}}$ , and the previous state of the slots. Slot attention uses standard dot-product attention [70] for computing the attention matrix  $\mathbf{A} \in \mathcal{R}^{N \times O}$ , *normalized over slots*. This normalization causes the slots to compete with each other, leading to a meaningful decomposition of the input scene. The slots are updated using a weighted combination of the input features  $\mathbf{H}$  and the computed attention matrix  $\mathbf{A}$ . Formally, this can be written as

$$\hat{\mathbf{S}} = \left( \frac{\mathbf{A}_{i,j}}{\sum_{l=1}^N \mathbf{A}_{l,j}} \right)_{i,j}^\top v(\mathbf{H}) \quad \text{with } \mathbf{A}(\mathbf{S}, \mathbf{H}) = \text{softmax} \left( \frac{k(\mathbf{H})q(\mathbf{S})^\top}{\sqrt{D}} \right), \quad (1)$$

where  $k$ ,  $q$ , and  $v$  are learnable linear functions for mapping the slots and input features to the same  $D$  dimensions. The updated set of slots  $\hat{\mathbf{S}}$  is fed into a decoder model to reconstruct the input. The decoder model can be a simple MLP [75], a transformer [66], or a diffusion model [31, 77]. Slot attention-based models are generally trained using the mean squared error (MSE) loss between the input and reconstructed input signal.

**Latent diffusion models (LDM)** [56] learn to generate an image by iteratively destructing the image by adding Gaussian noise at each time step. This noising process is called the “forward process”. The “reverse process”, or generation step, involves learning a neural network  $\epsilon_\theta$  that predicts the noise added in each forward diffusion step and removes the noise from the image. The parameters of  $\epsilon_\theta$  are learnt using

$$\mathcal{L}(\theta) = \mathbb{E}_{x_0, t \sim \mathcal{U}(0, T), \epsilon_t \sim \mathcal{N}(0, I)} [w(t) \|\epsilon_t - \epsilon_\theta(x_t; t, y)\|^2], \quad (2)$$

where  $t$  denotes the time step in the diffusion process and  $y$  is an additional conditioning signal such as text.  $w(t)$  denotes the weighting factor for each denoising step; in practice,  $w(t)$  is set to 1 [29] and  $x_0$  and  $x_t$  denote a low-dimensional representation of the image at time step 0 and  $t$  in the noising process and  $T$  denotes the total number of time steps. The most common choice for the denoising network  $\epsilon_\theta$  is a U-Net [57] with self and cross-attention layers at multiple resolutions.

### 4 Guided Latent Slot Diffusion (GLASS)

GLASS trains a slot attention module on the features of a DINOv2 [51] (encoder) model and uses a pre-trained Stable Diffusion (SD) model (decoder) to reconstruct the image. GLASS leverages the decoder model along with a pre-trained caption generation model [42] for creating a guidance signal (semantic masks) to guide slots.

A key design choice in GLASS is to learn the slot attention module in the space of generated images from a pre-trained diffusion model. This allows it to utilize the cross-attention layers in the U-Net [57] of a pre-trained diffusion model for obtaining the semantic mask for the generated image. Hertz et al. [26] were the first to show that cross-attention layers of the U-Net contain spatial information about objects and used it for localized editing of objects.

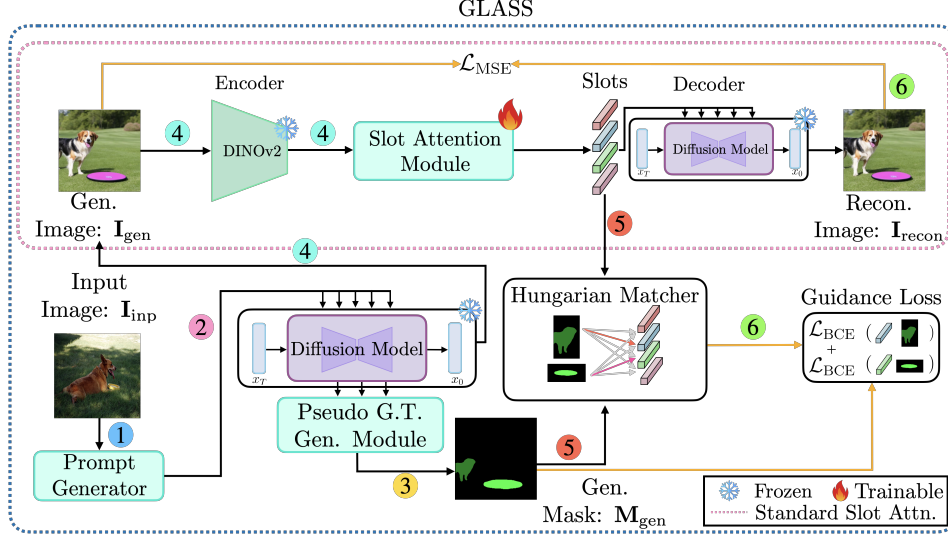


Figure 2: **Network architecture of GLASS.** ① The input image  $I_{\text{inp}}$  is fed to a prompt generator for generating a prompt  $\mathcal{P}$ , which is obtained by concatenating generated caption  $\mathcal{P}_{\text{cap}}$  and the extracted class label from  $\mathcal{P}_{\text{cap}}$ . ② A random noise vector, along with the generated prompt  $\mathcal{P}$ , is used to generate an image  $I_{\text{gen}}$  using a pre-trained diffusion module. ③ The cross-attention layers of the diffusion model, along with self-attention layers, are used in the pseudo ground-truth generation module to generate the semantic mask  $M_{\text{gen}}$  for  $I_{\text{gen}}$ . ④ The generated image is passed through an encoder model (DINOv2) followed by a slot attention module to generate slots. ⑤ The slots are matched with their corresponding object masks from  $M_{\text{gen}}$  using the Hungarian matcher module. ⑥ The slot attention module is trained end-to-end using the mean squared error between the reconstructed ( $I_{\text{recon}}$ ) and the generated ( $I_{\text{gen}}$ ) image and our *guidance loss* between the predicted mask from the slots and their matched object mask from  $M_{\text{gen}}$ . GLASS is trained on generated images only, the real images are only used for prompt generation.

**Conditional image generation.** Given an input image  $I_{\text{inp}}$ , we first pass it through a caption generator such as BLIP-2 [42] to generate a caption  $\mathcal{P}_{\text{cap}}$  that describes the input image. We extract the nouns from the generated caption using a part-of-speech (POS) tagger [4] and retain those nouns,  $\mathcal{C} = \{c_1, c_2 \dots c_k\}$ , that belong to the set of COCO’s class labels. We then create a prompt,  $\mathcal{P} = [\mathcal{P}_{\text{cap}}; \mathcal{C}]$ , by concatenating the generated caption and the extracted class labels. This prompt  $\mathcal{P}$  is fed into a text embedder, here CLIP [54], to obtain an embedding  $y \in \mathcal{R}^{U \times d_{\text{token}}}$ , where  $U$  is the number of tokens of dimension  $d_{\text{token}}$ . We then generate an image  $I_{\text{gen}}$  by sampling a random noise vector  $x_T$  from  $\mathcal{N}(0, I)$  and running the “reverse process” with  $y$  as a conditioning signal.

**Pseudo ground-truth generation module.** For extracting the cross-attention map at time  $t$  for layer  $l$  from the diffusion model, we create a new prompt consisting of a single token, namely one of the class tokens from  $\mathcal{C}$ . The cross-attention map for the target label can be computed using standard dot-product attention between the linear projections of the ground-truth class label embedding and the noisy image features  $x_t$  in a common  $d$ -dimensional space. This is done for each target class label in  $\mathcal{C}$ . The final cross-attention map  $A_{\text{CA}} \in [0, 1]^{H \times W \times C}$  is obtained by resizing and averaging the extracted cross-attention maps across different time steps and resolutions. Here,  $H$  and  $W$  are the size of the input embedding  $x_0$ ;  $C$  is the number of target classes. The obtained cross-attention maps are often noisy and require further refinement. A simple solution of using a single fixed threshold value for all classes produces poor results, and setting individual class thresholds becomes unfeasible as the number of classes increases. Recently, several works have addressed the problem of refining the cross-attention maps [37, 49, 76]. We follow [49] and use the self-attention maps for refining the cross-attention maps. In particular, the refined mask  $M_{\text{ref}}$  is obtained by exponentiating the self-attention map  $A_{\text{SA}} \in [0, 1]^{H \times W \times H \times W}$  and multiplying with the cross-attention map  $A_{\text{CA}}$  as described in [49]. The final semantic mask  $M_{\text{gen}}$  is obtained by taking the pixel-wise arg max of  $M_{\text{ref}}$  for all target class labels in  $\mathcal{C}$  to find which class is responsible for a given pixel. Finally, a range-based thresholding is used to classify each pixel as foreground or background.

**Slot matching.** Once the images  $\mathbf{I}_{\text{gen}}$  and their corresponding pseudo ground-truth semantic masks  $\mathbf{M}_{\text{gen}}$  are generated, we can use these semantic masks to guide the slots to bind to masks. First, we pass the generated image  $\mathbf{I}_{\text{gen}}$  through the encoder and the slot attention module to obtain a slot decomposition of the generated image. After this, we extract the predicted masks for each slot using the attention matrix  $\mathbf{A}$  from Equation (1) and resize them to the input resolution of the generated semantic mask  $\mathbf{M}_{\text{gen}}$ . We then assign each predicted mask to the components of the generated semantic masks. This is equivalent to solving a bipartite matching problem for which we use Hungarian matching [41]. Formally, given  $O$  slots and a semantic mask containing  $F$  segments, the binary matching matrix  $\mathbf{P} \in \{0, 1\}^{O \times F}$  can be computed using the Hungarian algorithm that minimizes the cost  $c_{i,j}$  of assigning slot  $o_i$  to segment  $m_j$  in the generated mask  $\mathbf{M}_{\text{gen}}$ . This optimization can be written as

$$\min_{\mathbf{P}} \sum_{i=1}^O \sum_{j=1}^F -c_{i,j} p_{i,j}, \quad (3)$$

where  $p_{i,j} \in \{0, 1\}$  indicates whether  $o_i$  is matched with segment  $m_j$ . The optimization is constrained to assign each slot to one and only one segment. The cost  $c_{i,j}$  is calculated using the mean Intersection over Union (IoU) between the predicted mask of slot  $o_i$  and segment  $m_j$  of the generated semantic mask  $\mathbf{M}_{\text{gen}}$ . The optimal assignment is the one that maximizes the overall mean IoU.

**Loss function.** Once the assignment is complete, our guided slot attention model is trained end-to-end using the mean squared error loss on the generated image  $\mathbf{I}_{\text{gen}}$  and reconstructed image  $\mathbf{I}_{\text{recon}}$  and our *guidance loss*, *i.e.* a binary cross-entropy loss between  $\mathbf{M}_{\text{gen}}$  and the predicted mask from the slots ( $\mathbf{A}(\mathbf{S}, \mathbf{H})$ ):

$$\mathcal{L} = \mathcal{L}_{\text{MSE}}(\mathbf{I}_{\text{gen}}, \mathbf{I}_{\text{recon}}) + \mathcal{L}_{\text{BCE}}(\mathbf{M}_{\text{gen}}, \mathbf{A}(\mathbf{S}, \mathbf{H})). \quad (4)$$

The binary cross-entropy loss  $\mathcal{L}_{\text{BCE}}$  is only computed on the matched slots. This enables our model to implicitly learn to count the number of objects and assign only one slot to one object at training time. Fig. 2 shows our full architecture and illustrates each step.

Our novel guidance method helps the slots to better aggregate the features from the encoder model, leading to better-learned slot embeddings. Also, only using slots matched to pseudo ground-truth segments in the guidance loss helps the model implicitly learn the number of objects in a scene and regularizes the slot embeddings to be more object-centric.

## 5 Experiments

The main focus of our work is to address the part-whole hierarchy ambiguity plaguing object-centric learning methods on real-world datasets. To assess this, we test the efficacy of our proposed method, GLASS, on object discovery for real images. Additionally, we show that other tasks, such as object-level property prediction and conditional image generation, benefit from slots binding to objects instead of parts. Our method uses generated captions and can be (loosely) considered a weakly supervised method. Thus, we test it against other weakly supervised OCL methods. To that end, we also propose a variant of GLASS termed GLASS<sup>†</sup>, which uses ground-truth class labels associated with the input image instead of the generated caption as done in GLASS.

**Implementation details.** GLASS uses a DINOv2 [51] model with ViT-B and a patch size of 14 as the encoder model, and a Stable Diffusion (SD) v2.1 [56] model as its decoder model. GLASS is trained on images generated from the SD model. We use the ground-truth images to generate captions using BLIP-2 and then generate a training image conditioned on the prompt, which is composed of the generated caption and classes extracted from it. We used the same number of training samples in the generated dataset as in the original dataset, *i.e.* approx. 118K for COCO and approx. 12K for the VOC dataset. We trained GLASS for 500K (COCO-generated) and 250K (VOC-generated) steps using the Adam [39] optimizer with a constant learning rate of  $2e-5$ .

**Datasets.** As in previous work [31, 63, 77], we report all our results on the VOC [20] and COCO [43] datasets, which consist of 20 and 80 foreground classes, respectively. Both these datasets are multi-object, serve as popular benchmarks for object discovery, and have recently been used to evaluate the performance of various object-centric learning methods on real-world images [31, 63, 77].

Table 2: **Comparison for object discovery across all classes of models.** We compare our method against language-based segmentation models (top partition), weakly-supervised models (middle partition), and OCL models (bottom partition) for the object discovery task. Downstream Tasks denote a model’s capability for solving the following tasks: OD – object discovery, PP – object-level property prediction, and CG – conditional generation. Input denotes the input signal the model trains on, where  $\mathcal{I}$  – image,  $\mathcal{C}$  – captions, and  $\mathcal{L}$  – image-level labels. The best value is highlighted in **red**, the second best in **blue**. We show the relative improvement (in parentheses) of GLASS compared to the best OCL method. Our method outperforms all models on the COCO dataset and is comparable to the best model on the VOC dataset (ToCo [59]).

Model	Downstream Tasks	Input	Pre-Trained Models	mIoU	
				COCO	VOC
MaskCLIP [84] ECCV’22	OD	$\mathcal{I} + \mathcal{C}$	CLIP	23.6	38.8
SegCLIP [46] ICML’23	OD	$\mathcal{I} + \mathcal{C}$	CLIP	24.7	52.6
CLIPPy [55] ICCV’23	OD	$\mathcal{I} + \mathcal{C}$	CLIP	–	52.2
OVSeg [80] CVPR’23	OD	$\mathcal{I} + \mathcal{C}$	CLIP	20.4	53.8
OVDiff [36] CVPR-W’24	OD	$\mathcal{I} + \mathcal{C}$	SD + DINO + CLIP	30.1	67.1
DiffuMask [76] NeurIPS’23	OD	$\mathcal{I} + \mathcal{C}$	SD + CLIP + Aff. Net[1]	–	57.4
Dataset Diffusion [49] NeurIPS’23	OD	$\mathcal{I} + \mathcal{C}$	SD + BLIP-2	34.2	64.8
IStage [2] CVPR’20	OD	$\mathcal{I} + \mathcal{L}$	–	–	62.7
AFA [58] CVPR’22	OD	$\mathcal{I} + \mathcal{L}$	–	38.9	66.0
ToCo [59] CVPR’23	OD	$\mathcal{I} + \mathcal{L}$	–	41.3	<b>69.8</b>
DINOSAUR-MLP [63] ICLR’23	OD + PP	$\mathcal{I}$	DINO	32.1	41.0
DINOSAUR-Transformer [63] ICLR’23	OD + PP	$\mathcal{I}$	DINO	40.6	47.5
StableLSD [31] NeurIPS’23	OD + PP + CG	$\mathcal{I}$	SD + DINOv2	29.5	32.9
GLASS <sup>†</sup> (ours)	OD + PP + CG	$\mathcal{I} + \mathcal{L}$	SD + DINOv2	<b>42.3</b> (+4.1%)	<b>67.8</b> (+42.7%)
GLASS (ours)	OD + PP + CG	$\mathcal{I} + \mathcal{C}$	SD + DINOv2 + BLIP-2	<b>43.7</b> (+9.1%)	64.0 (+34.7%)

## 5.1 Object discovery

The standard way to test if the slots bind to objects instead of parts is to test the performance of these models for object discovery. We compare GLASS against three classes of models: (i) Object-centric methods as GLASS is primarily a slot attention-based method. (ii) Language-based segmentation methods as GLASS uses language cues in the form of generated captions from the BLIP-2 model for generating the guiding signal. (iii) Weakly-supervised segmentation methods as GLASS can be considered a weakly-supervised method since it utilizes generated captions. We evaluate all three classes of methods using the standard mean Intersection over Union (mIoU) metric between the predicted masks from the slots, which are computed using the attention weights,  $\mathbf{A}(\mathbf{S}, \mathbf{H})$  as defined in Equation (1), and ground-truth semantic masks. Table 2 shows that our method outperforms all object-centric learning, language-based, and weakly-supervised models on the COCO dataset. For the VOC dataset, GLASS and GLASS<sup>†</sup> are only slightly surpassed by ToCo [59]. However, ToCo is a weakly-supervised model that can only perform segmentation, while our method can perform multiple tasks. We believe the improvement in GLASS compared to other models that use foundational models methods is due to the interplay of features between the different foundational models. GLASS aggregates features from a foundation model (DINOv2 [51]) like StableLSD [31] and DINOSAUR [63], but unlike these models, the feature aggregation is guided by diffusion-based features. Our claim is bolstered by the observation that GLASS outperforms models such as Dataset Diffusion [49] and OVDiff [36] even though these models, like GLASS, use Stable Diffusion features for creating pseudo-labels. These results show the effectiveness of using guidance signals combined with slot attention compared to other classes of models. The difference in performance between VOC and COCO is due to VOC being a simpler dataset containing many images with a single object.

**Comparison to OCL methods.** Our method is primarily an OCL method, so we next evaluate our model against various object-centric models. We use the standard object discovery metrics popular in the OCL literature [31, 63, 77], like mean Best Overlap over instance level masks (mBO<sub>i</sub>) and over class-level masks (mBO<sub>c</sub>). We also report the results for the Correct Localization (CorLoc) [72] and Detection Rate (DetRate) metrics. CorLoc computes the fraction of images where at least one ground-truth class was correctly localized (IoU > 0.5), and DetRate measures the number of ground-truth classes with IoU greater than a certain threshold (here 0.5) with the predicted masks. Table 3 shows that GLASS outperforms all previous OCL methods across all metrics by a wide margin.

Table 3: **Comparison between OCL methods for object discovery.** GLASS and GLASS<sup>†</sup> outperform all other SOTA OCL methods on the object discovery metrics. \* numbers are taken from [77].

Model	COCO				VOC			
	mBO <sub>i</sub> ↑	mBO <sub>c</sub> ↑	CorLoc↑	DetRate↑	mBO <sub>i</sub> ↑	mBO <sub>c</sub> ↑	CorLoc↑	DetRate↑
SA* [45] NeurIPS'20	17.2	19.2	–	–	24.6	24.9	–	–
SLATE* [65] ICLR'22	29.1	33.6	–	–	35.9	41.5	–	–
DINOSAUR-MLP [63] ICLR'23	28.07	32.14	57.04	18.0	39.72	41.18	57.41	28.36
DINOSAUR-Trans. [63] ICLR'23	31.60	39.70	72.96	28.49	43.15	51.20	70.53	38.44
SlotDiffusion* [77] NeurIPS'23	31.0	35.0	–	–	50.4	55.3	–	–
StableLSD [31] NeurIPS'23	25.85	30.04	48.46	14.11	30.41	33.08	20.28	8.11
GLASS <sup>†</sup> (ours)	<u>34.35</u>	<u>45.23</u>	<b>94.48</b>	<u>35.26</u>	<b>60.44</b>	<b>68.40</b>	<b>98.96</b>	<b>66.13</b>
GLASS (ours)	<b>35.27</b>	<b>46.28</b>	<u>91.78</u>	<b>36.11</b>	<u>58.07</u>	<u>65.47</u>	<u>96.61</u>	<u>62.69</u>

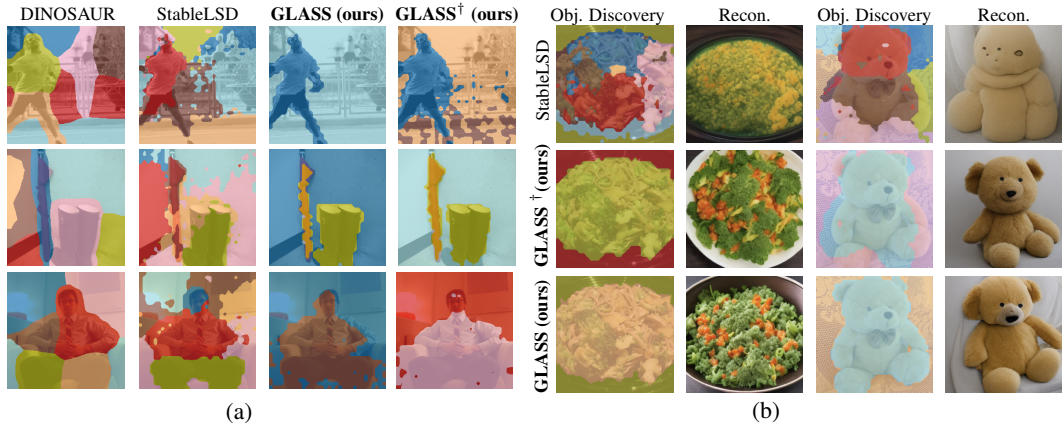


Figure 3: (a) **Qualitative comparison for object discovery.** GLASS and GLASS<sup>†</sup> can decompose an image at an object level and do not split an object into its parts. Also they have cleaner boundaries for the foreground objects compared to DINOSAUR and StableLSD. (b) **Qualitative comparison for conditional image generation.** GLASS and GLASS<sup>†</sup> not only learn to decompose scenes meaningfully, but this decomposition also leads to higher fidelity conditional image generation.

Fig. 3a shows qualitative results for object discovery compared to DINOSAUR and StableLSD. The qualitative results show that GLASS performs a decomposition of the scene in a more object-centric way with sharper boundaries, no object splitting, and cleaner background segmentation.

**Comparison to weakly-supervised OCL.** We next compare GLASS against existing weakly supervised solutions proposed in the literature to guide slots to bind to objects. We compare our method against two weakly-supervised variants of StableLSD: (i) StableLSD-BBox – This method uses the bounding-box information associated with each object for initializing the objects. This form of guidance has been previously used in [40] and has proven very effective. (ii) StableLSD-Dynamic – Instead of having a fixed number of slots for each scene, this method dynamically assigns each scene the number of slots equal to the number of objects present in the scene. This technique was useful [85] for addressing the issue of part-whole hierarchy ambiguity, leading to better object discovery performance. We compare both these methods against GLASS and GLASS<sup>†</sup>. We choose StableLSD for comparison since it is closest to our model in terms of the downstream tasks it can perform (see Table 1). As seen in Fig. 4a, all weakly-supervised variants of StableLSD outperform StableLSD by a healthy margin. *Importantly*, GLASS outperforms both weakly-supervised methods even though it uses a weaker supervision signal compared to bounding box information.

## 5.2 Additional tasks

**Conditional generation.** An essential aspect of slot attention-based models is that the slots can conditionally generate a scene. To evaluate how well our model can reconstruct the input, we use the FID metric [27] between 1024 generated and real images. We compare GLASS against the StableLSD model (as this is the only OCL model capable of reconstructing the real-world images, see Table 1). To reconstruct the images, we decompose the input image into a set of slots using the slot-

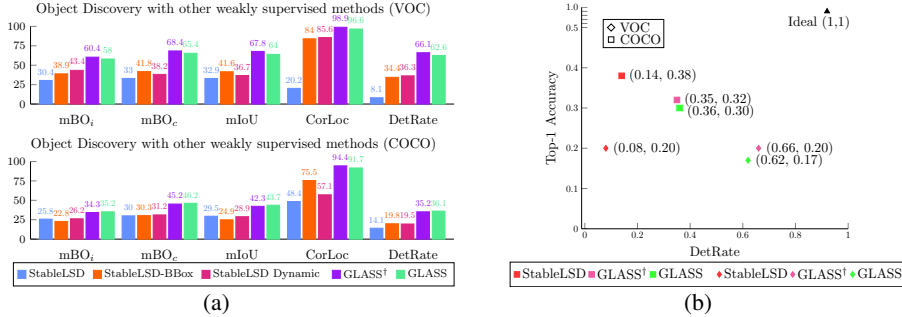


Figure 4: (a) **Comparison with WSL methods**, *i.e.* weakly-supervised variants of StableLSD. GLASS outperforms StableLSD-Dynamic on all object discovery metrics. Also, GLASS is better than StableLSD-BBox on all metrics even though GLASS uses a much weaker supervision signal (captions) compared to bounding box information. (b) **Object-level property prediction**. An ideal model should have a high detection rate and accuracy. GLASS and GLASS<sup>†</sup> have a slightly lower (approx. -2%) accuracy drop but have a higher increase in detection rate compared to StableLSD. Here,  $\square$  and  $\diamond$  show the results for the COCO and VOC datasets, respectively.

attention module, which acts as a conditioning signal to the decoder. GLASS outperforms StableLSD by approx. +2% and approx. +7% on the VOC and COCO datasets (see Table 4), respectively. Our method establishes a new SOTA among OCL methods in terms of the FID metric for scene reconstruction of real images. These results indicate that the learned slot embeddings of GLASS can reconstruct the scene with much higher fidelity than StableLSD (see Fig. 3b). The improvement comes from using a better conditioning signal, as the diffusion models are frozen for all models.

**Object-level property prediction** assesses the representation quality of the slots. This task involves predicting object properties, such as class labels for input images from the learned slot embeddings. We follow the experimental design of Dittadi et al. [14] and train a single-layer MLP model for label prediction where the ground-truth labels and predicted labels from each slot are mapped to each other based on the mIoU between the ground-truth and predicted semantic mask from the slots. For more details, please see Appendix A.2. We report the Top-1 accuracy alongside the detection rate metric in Fig. 4b. An ideal model should be highly accurate, and the slot should represent the full object, not just its parts. GLASS and GLASS<sup>†</sup> are slightly worse (approx. -2%) than StableLSD for the property prediction task but GLASS outperforms StableLSD by  $\geq 26\%$  on DetRate. StableLSD’s slots learn informative embeddings but are poorly localized compared to GLASS’s slots, which localize the object better and are comparable to StableLSD for the property prediction task. Moreover, we found GLASS to have higher accuracy than StableLSD with increasing threshold values used for IoU matching ( $\geq 0.7$ ).

Table 4: **Conditional generation** Comparison between StableLSD, GLASS<sup>†</sup>, and GLASS for the conditional generation task.

Model	FID $\downarrow$	
	VOC	COCO
StableLSD [31] NeurIPS’23	65.12	78.47
GLASS <sup>†</sup> (ours)	65.15	72.25 (+6.8)
GLASS (ours)	63.70 (+2.18)	73.06

## 6 Conclusion

We present GLASS, a novel object-centric learning method that learns in the space of generated images from a pre-trained diffusion model. GLASS uses a pre-trained Stable Diffusion (SD) model as a decoder, for decoding the slots, and as a guidance signal generator. We utilize the prior knowledge about objectness in the SD model to guide slots for learning better object-centric representations. GLASS establishes a new SOTA for OCL methods w.r.t. object discovery and conditional image generation tasks while being comparable for object-level property prediction. GLASS outperforms SOTA weakly-supervised methods and language-based segmentation models on the COCO dataset and is only behind ToCo [59] on the VOC dataset for object discovery task. Our work shows that learning in the space of generated images and using additional inductive biases in OCL methods binds slots to more human-interpretable notions of objects.

## Acknowledgments

This project has received funding from the European Research Council (ERC) under the European Union’s Horizon 2020 research and innovation program (grant agreement No. 866008). The project has also been supported in part by the State of Hesse through the cluster projects “The Third Wave of Artificial Intelligence (3AI)” and “The Adaptive Mind (TAM).”

## Broader impact statement

Our method learns to decompose input images into objects that can be used for various downstream tasks. The method can enable manipulating the input scene at the object level, which can help us better understand and evaluate the behavior of the downstream model. Our method learns to decompose a scene more effectively and can generate realistic-looking objects. Our model’s generative capability allows manipulation at the object level, *i.e.* nefarious actors could use it to insert people and objects in other places. This adds to the common concerns about deepfakes. Possible safeguards are required for using these models responsibly; methods like [47] can be used for watermarking and identifying if an image has been manipulated. Moreover, we advocate for more stringent policies regarding using these models for commercial purposes.

## References

- [1] Jiwoon Ahn and Suha Kwak. Learning pixel-level semantic affinity with image-level supervision for weakly supervised semantic segmentation. In *CVPR*, pages 4981–4990, 2018. 7
- [2] Nikita Araslanov and Stefan Roth. Single-stage semantic segmentation from image labels. In *CVPR*, pages 4253–4262, 2020. 2, 3, 7
- [3] Rim Assouel, Pau Rodriguez, Perouz Taslakian, David Vazquez, and Yoshua Bengio. Object-centric compositional imagination for visual abstract reasoning. In *ICLR Workshop on the Elements of Reasoning: Objects, Structure and Causality*, 2022. 1
- [4] Steven Bird and Edward Loper. NLTK: The natural language toolkit. In *Proceedings of the ACL Interactive Poster and Demonstration Sessions*, 2004. 5
- [5] Ondrej Biza, Robert Platt, Jan-Willem van de Meent, Lawson L.S. Wong, and Thomas Kipf. Binding actions to objects in world models. In *ICLR Workshop on the Elements of Reasoning: Objects, Structure and Causality*, 2022. 1
- [6] Christopher P Burgess, Loic Matthey, Nicholas Watters, Rishabh Kabra, Irina Higgins, Matt Botvinick, and Alexander Lerchner. MONet: Unsupervised scene decomposition and representation. *arXiv:1901.11390 [cs.CV]*, 2019. 3
- [7] Mathilde Caron, Ishan Misra, Julien Mairal, Priya Goyal, Piotr Bojanowski, and Armand Joulin. Unsupervised learning of visual features by contrasting cluster assignments. *NeurIPS*, pages 9912–9924, 2020. 3
- [8] Mathilde Caron, Hugo Touvron, Ishan Misra, Hervé J’egou, Julien Mairal, Piotr Bojanowski, and Armand Joulin. Emerging properties in self-supervised vision transformers. In *ICCV*, pages 9650–9660, 2021. 16
- [9] Junbum Cha, Jonghwan Mun, and Byungseok Roh. Learning to generate text-grounded mask for open-world semantic segmentation from only image-text pairs. In *CVPR*, pages 11165–11174, 2023. 3
- [10] Jang Hyun Cho, Utkarsh Mall, Kavita Bala, and Bharath Hariharan. PiCIE: Unsupervised semantic segmentation using invariance and equivariance in clustering. In *CVPR*, pages 16794–16804, 2021. 3
- [11] Kyunghyun Cho, Bart van Merriënboer, Caglar Gulcehre, Dzmitry Bahdanau, Fethi Bougares, Holger Schwenk, and Yoshua Bengio. Learning phrase representations using rnn encoder–decoder for statistical machine translation. In *EMNLP*, 2014. 4

- [12] Eric Crawford and Joelle Pineau. Spatially invariant unsupervised object detection with convolutional neural networks. In *AAAI*, pages 3412–3420, 2019. 3
- [13] Zheng Ding, Jieke Wang, and Zhuowen Tu. Open-vocabulary universal image segmentation with MaskCLIP. In *ICML*, 2023. 3
- [14] Andrea Dittadi, Samuele Papa, Michele De Vita, Bernhard Schölkopf, Ole Winther, and Francesco Locatello. Generalization and robustness implications in object-centric learning. In *ICML*, pages 5221–5285, 2021. 1, 9
- [15] Carl Doersch, Abhinav Gupta, and Alexei A Efros. Unsupervised visual representation learning by context prediction. In *ICCV*, pages 1422–1430, 2015. 3
- [16] Cathrin Elich, Martin R. Oswald, Marc Pollefeys, and Joerg Stueckler. Weakly supervised learning of multi-object 3D scene decompositions using deep shape priors. *Comput. Vis. Image Und.*, page 103440, 2022. 4
- [17] Gamaleldin F. Elsayed, Aravindh Mahendran, Sjoerd van Steenkiste, Klaus Greff, Michael C. Mozer, and Thomas Kipf. SAVi++: Towards end-to-end object-centric learning from real-world videos. In *NeurIPS*, pages 28940–28954, 2022. 4
- [18] Martin Engelcke, Adam R. Kosiorek, Oiwi Parker Jones, and Ingmar Posner. GENESIS: Generative scene inference and sampling with object-centric latent representations. In *ICLR*, 2020. 3
- [19] S.M. Ali Eslami, Nicolas Heess, Theophane Weber, Yuval Tassa, David Szepesvari, Koray Kavukcuoglu, and Geoffrey E. Hinton. Attend, infer, repeat: Fast scene understanding with generative models. *NIPS*, 2016. 3
- [20] Mark Everingham, Luc Van Gool, Christopher K.I. Williams, John Winn, and Andrew Zisserman. The pascal visual object classes (VOC) challenge. *Int. J. Comput. Vision*, pages 303–338, 2010. 1, 6
- [21] Lijie Fan, Kaifeng Chen, Dilip Krishnan, Dina Katabi, Phillip Isola, and Yonglong Tian. Scaling laws of synthetic images for model training... for now. *arXiv:2312.04567 [cs.CV]*, 2023. 2
- [22] Klaus Greff, Raphaël Lopez Kaufman, Rishabh Kabra, Nick Watters, Christopher Burgess, Daniel Zoran, Loic Matthey, Matthew Botvinick, and Alexander Lerchner. Multi-object representation learning with iterative variational inference. In *ICML*, pages 2424–2433, 2019. 3
- [23] Klaus Greff, Sjoerd Van Steenkiste, and Jürgen Schmidhuber. On the binding problem in artificial neural networks. *arXiv:2012.05208 [cs.NE]*, 2020. 1, 3
- [24] Klaus Greff, Francois Belletti, Lucas Beyer, Carl Doersch, et al. Kubric: A scalable dataset generator. In *CVPR*, pages 3749–3761, 2022. 1, 3
- [25] Mark Hamilton, Zhoutong Zhang, Bharath Hariharan, Noah Snavely, and William T. Freeman. Unsupervised semantic segmentation by distilling feature correspondences. In *ICLR*, 2022. 3
- [26] Amir Hertz, Ron Mokady, Jay Tenenbaum, Kfir Aberman, Yael Pritch, and Daniel Cohen-Or. Prompt-to-prompt image editing with cross attention control. In *ICLR*, 2023. 4
- [27] Martin Heusel, Hubert Ramsauer, Thomas Unterthiner, Bernhard Nessler, and Sepp Hochreiter. GANs trained by a two time-scale update rule converge to a local nash equilibrium. *NIPS*, 30, 2017. 8
- [28] Geoffrey Hinton. Some demonstrations of the effects of structural descriptions in mental imagery. *Cognitive Science*, pages 231–250, 1979. 2
- [29] Jonathan Ho, Ajay Jain, and Pieter Abbeel. Denoising diffusion probabilistic models. *NeurIPS*, pages 6840–6851, 2020. 4
- [30] Baoxiong Jia, Yu Liu, and Siyuan Huang. Improving object-centric learning with query optimization. In *ICLR*, 2022. 1

- [31] Jindong Jiang, Fei Deng, Gautam Singh, and Sungjin Ahn. Object-centric slot diffusion. In *NeurIPS*, 2023. 1, 2, 3, 4, 6, 7, 8, 9
- [32] Justin Johnson, Bharath Hariharan, Laurens Van Der Maaten, Li Fei-Fei, C. Lawrence Zitnick, and Ross Girshick. CLEVR: A diagnostic dataset for compositional language and elementary visual reasoning. In *CVPR*, pages 2901–2910, 2017. 1, 3
- [33] Rishabh Kabra, Daniel Zoran, Goker Erdogan, Loic Matthey, Antonia Creswell, Matt Botvinick, Alexander Lerchner, and Chris Burgess. SIMONe: View-invariant, temporally-abstracted object representations via unsupervised video decomposition. *NeurIPS*, pages 20146–20159, 2021. 3
- [34] Daniel Kahneman, Anne Treisman, and Brian J. Gibbs. The reviewing of object files: Object-specific integration of information. *Cognitive psychology*, pages 175–219, 1992. 1
- [35] Laurynas Karazija, Iro Laina, and Christian Rupprecht. ClevrTex: A texture-rich benchmark for unsupervised multi-object segmentation. In *NeurIPS Datasets and Benchmarks Track*, 2021. 1, 3
- [36] Laurynas Karazija, Iro Laina, Andrea Vedaldi, and Christian Rupprecht. Diffusion models for zero-shot open-vocabulary segmentation. *arXiv:2306.09316 [cs.CV]*, 2023. 2, 3, 7
- [37] Aliasghar Khani, Saeid Asgari Taghanaki, Aditya Sanghi, Ali Mahdavi Amiri, and Ghassan Hamarneh. SLiMe: Segment like me. *arXiv:2309.03179 [cs.CV]*, 2023. 3, 5
- [38] Dongwon Kim, Namyup Kim, Cuiling Lan, and Suha Kwak. Shatter and gather: Learning referring image segmentation with text supervision. In *ICCV*, pages 15547–15557, 2023. 4
- [39] Diederik P. Kingma and Jimmy Ba. Adam: A method for stochastic optimization. In *ICLR*, 2014. 6
- [40] Thomas Kipf, Gamaleldin F. Elsayed, Aravindh Mahendran, Austin Stone, Sara Sabour, Georg Heigold, Rico Jonschkowski, Alexey Dosovitskiy, and Klaus Greff. Conditional object-centric learning from video. In *ICLR*, 2022. 2, 3, 4, 8, 16
- [41] Harold W. Kuhn. The hungarian method for the assignment problem. *Naval research logistics quarterly*, pages 83–97, 1955. 6
- [42] Junnan Li, Dongxu Li, Silvio Savarese, and Steven Hoi. BLIP-2: Bootstrapping language-image pre-training with frozen image encoders and large language models. In *ICML*, 2023. 4, 5
- [43] Tsung-Yi Lin, Michael Maire, Serge Belongie, James Hays, Pietro Perona, Deva Ramanan, Piotr Dollár, and C. Lawrence Zitnick. Microsoft COCO: Common objects in context. In *ECCV*, pages 740–755, 2014. 1, 6
- [44] Shilong Liu, Zhaoyang Zeng, Tianhe Ren, et al. Grounding DINO: Marrying DINO with grounded pre-training for open-set object detection. *arXiv:2303.05499 [cs.CV]*, 2023. 19
- [45] Francesco Locatello, Dirk Weissenborn, Thomas Unterthiner, Aravindh Mahendran, Georg Heigold, Jakob Uszkoreit, Alexey Dosovitskiy, and Thomas Kipf. Object-centric learning with slot attention. In *NeurIPS*, pages 11525–11538, 2020. 1, 3, 4, 8
- [46] Huaishao Luo, Junwei Bao, Youzheng Wu, Xiaodong He, and Tianrui Li. SegCLIP: Patch aggregation with learnable centers for open-vocabulary semantic segmentation. In *ICML*, pages 23033–23044, 2023. 2, 3, 7
- [47] Xiyang Luo, Michael Goebel, Elnaz Barshan, and Feng Yang. LECA: A learned approach for efficient cover-agnostic watermarking. *arXiv:2206.10813 [cs.MM]*, 2022. 10
- [48] Jishnu Mukhoti, Tsung-Yu Lin, Omid Poursaeed, Rui Wang, Ashish Shah, Philip H.S. Torr, and Ser-Nam Lim. Open vocabulary semantic segmentation with patch aligned contrastive learning. In *CVPR*, pages 19413–19423, 2023. 3
- [49] Quang Ho Nguyen, Truong Tuan Vu, Anh Tuan Tran, and Khoi Nguyen. Dataset Diffusion: Diffusion-based synthetic data generation for pixel-level semantic segmentation. In *NeurIPS*, 2023. 3, 5, 7

- [50] Mehdi Noroozi and Paolo Favaro. Unsupervised learning of visual representations by solving jigsaw puzzles. In *ECCV*, pages 69–84, 2016. 3
- [51] Maxime Oquab, Timothée Darcet, Théo Moutakanni, Huy Vo, Marc Szafraniec, Vasil Khalidov, Pierre Fernandez, Daniel Haziza, Francisco Massa, Alaaeldin El-Nouby, et al. DINOv2: Learning robust visual features without supervision. *arXiv:2304.07193 [cs.CV]*, 2023. 4, 6, 7, 15
- [52] Koutilya Pnvr, Bharat Singh, Pallabi Ghosh, Behjat Siddiquie, and David Jacobs. LD-ZNet: A latent diffusion approach for text-based image segmentation. In *ICCV*, pages 4157–4168, 2023. 3
- [53] Senthil Purushwalkam and Abhinav Gupta. Demystifying contrastive self-supervised learning: Invariances, augmentations and dataset biases. *NeurIPS*, pages 3407–3418, 2020. 3
- [54] Alec Radford, Jong Wook Kim, Chris Hallacy, et al. Learning transferable visual models from natural language supervision. In *ICML*, pages 8748–8763, 2021. 2, 3, 5
- [55] Kanchana Ranasinghe, Brandon McKinzie, Sachin Ravi, Yinfei Yang, Alexander Toshev, and Jonathon Shlens. Perceptual grouping in contrastive vision-language models. In *ICCV*, pages 5571–5584, 2023. 2, 3, 7
- [56] Robin Rombach, Andreas Blattmann, Dominik Lorenz, Patrick Esser, and Björn Ommer. High-resolution image synthesis with latent diffusion models. In *CVPR*, pages 10684–10695, 2022. 1, 2, 3, 4, 6, 15
- [57] Olaf Ronneberger, Philipp Fischer, and Thomas Brox. U-Net: Convolutional networks for biomedical image segmentation. In *MICCAI*, pages 234–241, 2015. 4
- [58] Lixiang Ru, Yibing Zhan, Baosheng Yu, and Bo Du. Learning affinity from attention: End-to-end weakly-supervised semantic segmentation with transformers. In *CVPR*, pages 16846–16855, 2022. 2, 3, 7
- [59] Lixiang Ru, Heliang Zheng, Yibing Zhan, and Bo Du. Token contrast for weakly-supervised semantic segmentation. In *CVPR*, pages 3093–3102, 2023. 2, 3, 7, 9
- [60] Mert Bülent Sarıyıldız, Karteek Alahari, Diane Larlus, and Yannis Kalantidis. Fake it till you make it: Learning transferable representations from synthetic ImageNet clones. In *CVPR*, pages 8011–8021, 2023. 2
- [61] Bernhard Schölkopf, Francesco Locatello, Stefan Bauer, Nan Rosemary Ke, Nal Kalchbrenner, Anirudh Goyal, and Yoshua Bengio. Toward causal representation learning. *Proceedings of the IEEE*, pages 612–634, 2021. 1
- [62] Christoph Schuhmann, Romain Beaumont, Richard Vencu, et al. LAION-5B: An open large-scale dataset for training next generation image-text models. *NeurIPS*, 35:25278–25294, 2022. 2
- [63] Maximilian Seitzer, Max Horn, Andrii Zadaianchuk, et al. Bridging the gap to real-world object-centric learning. In *ICLR*, 2022. 1, 2, 3, 6, 7, 8, 17, 19
- [64] Piyush Sharma, Nan Ding, Sebastian Goodman, and Radu Soricut. Conceptual captions: A cleaned, hypernymed, image alt-text dataset for automatic image captioning. In *ACL*, pages 2556–2565, 2018. 2
- [65] Gautam Singh, Fei Deng, and Sungjin Ahn. Illiterate DALL-E learns to compose. In *ICLR*, 2021. 1, 8
- [66] Gautam Singh, Yi-Fu Wu, and Sungjin Ahn. Simple unsupervised object-centric learning for complex and naturalistic videos. *NeurIPS*, pages 18181–18196, 2022. 1, 3, 4
- [67] Krishnakant Singh, Thanush Navaratnam, Jannik Holmer, Simone Schaub-Meyer, and Stefan Roth. Is synthetic data all we need? benchmarking the robustness of models trained with synthetic images. In *CVPR 2024 Workshop SyntaGen: Harnessing Generative Models for Synthetic Visual Datasets*, 2024. 2

- [68] Matthias Tangemann, Steffen Schneider, Julius Von Kügelgen, Francesco Locatello, Peter Vincent Gehler, Thomas Brox, Matthias Kuemmerer, Matthias Bethge, and Bernhard Schölkopf. Unsupervised object learning via common fate. In *CLear*, 2023. 4
- [69] Yonglong Tian, Lijie Fan, Phillip Isola, Huiwen Chang, and Dilip Krishnan. StableRep: Synthetic images from text-to-image models make strong visual representation learners. *NeurIPS*, 36, 2024. 2
- [70] Ashish Vaswani, Noam Shazeer, Niki Parmar, Jakob Uszkoreit, Llion Jones, Aidan N. Gomez, Łukasz Kaiser, and Illia Polosukhin. Attention is all you need. *NIPS*, 2017. 4, 16
- [71] Pascal Vincent, Hugo Larochelle, Yoshua Bengio, and Pierre-Antoine Manzagol. Extracting and composing robust features with denoising autoencoders. In *ICML*, pages 1096–1103, 2008. 3
- [72] Huy V. Vo, Patrick Pérez, and Jean Ponce. Toward unsupervised, multi-object discovery in large-scale image collections. In *ECCV*, pages 779–795, 2020. 7
- [73] Johan Wagemans, James H. Elder, Michael Kubovy, Stephen E. Palmer, Mary A. Peterson, Manish Singh, and Rüdiger Von der Heydt. A century of Gestalt psychology in visual perception: I. Perceptual grouping and figure–ground organization. *Psychological bulletin*, page 1172, 2012. 2
- [74] Johan Wagemans, Jacob Feldman, Sergei Gepshtein, Ruth Kimchi, James R. Pomerantz, Peter A. Van der Helm, and Cees Van Leeuwen. A century of Gestalt psychology in visual perception: II. Conceptual and theoretical foundations. *Psychological bulletin*, page 1218, 2012. 2
- [75] Nick Watters, Loic Matthey, Chris P. Burgess, and Alexander Lerchner. Spatial broadcast decoder: A simple architecture for disentangled representations in VAEs. In *ICLR Workshop on Learning from Limited Labeled Data*, 2019. 4
- [76] Weijia Wu, Yuzhong Zhao, Mike Zheng Shou, Hong Zhou, and Chunhua Shen. DiffuMask: Synthesizing images with pixel-level annotations for semantic segmentation using diffusion models. In *ICCV*, pages 1206–1217, 2023. 2, 3, 5, 7
- [77] Ziyi Wu, Jingyu Hu, Wuyue Lu, Igor Gilitschenski, and Animesh Garg. SlotDiffusion: Object-centric generative modeling with diffusion models. In *NeurIPS*, 2023. 1, 2, 3, 4, 6, 7, 8
- [78] Jiarui Xu, Shalini De Mello, Sifei Liu, Wonmin Byeon, Thomas Breuel, Jan Kautz, and Xiaolong Wang. GroupViT: Semantic segmentation emerges from text supervision. In *CVPR*, pages 18134–18144, 2022. 3
- [79] Jiarui Xu, Sifei Liu, Arash Vahdat, Wonmin Byeon, Xiaolong Wang, and Shalini De Mello. Open-vocabulary panoptic segmentation with text-to-image diffusion models. In *CVPR*, pages 2955–2966, 2023. 3
- [80] Jilan Xu, Junlin Hou, Yuejie Zhang, Rui Feng, Yi Wang, Yu Qiao, and Weidi Xie. Learning open-vocabulary semantic segmentation models from natural language supervision. In *CVPR*, pages 2935–2944, 2023. 3, 7
- [81] Yafei Yang and Bo Yang. Promising or elusive? Unsupervised object segmentation from real-world single images. *NeurIPS*, pages 4722–4735, 2022. 3
- [82] Liheng Zhang, Guo-Jun Qi, Liqiang Wang, and Jiebo Luo. AET vs. AED: Unsupervised representation learning by auto-encoding transformations rather than data. In *CVPR*, pages 2547–2555, 2019. 3
- [83] Richard Zhang, Phillip Isola, and Alexei A Efros. Colorful image colorization. In *ECCV*, pages 649–666, 2016. 3
- [84] Chong Zhou, Chen Change Loy, and Bo Dai. Extract free dense labels from clip. In *ECCV*, pages 696–712, 2022. 2, 3, 7
- [85] Roland S Zimmermann, Sjoerd van Steenkiste, Mehdi SM Sajjadi, Thomas Kipf, and Klaus Greff. Sensitivity of slot-based object-centric models to their number of slots. *arXiv:2305.18890 [cs.CV]*, 2023. 3, 4, 8

## A Appendix

In this appendix, we give additional details and results for our work. Specifically, we provide the following:

1. Training details for GLASS in Appendix [A.1](#)
2. Training details for the object-level property prediction task in Appendix [A.2](#)
3. Comparison with other guiding signals in Appendix [A.3](#)
4. Guidance for other architectures in Appendix [A.4](#)
5. Additional qualitative results for object discovery in Appendix [A.5](#)
6. Additional qualitative results for conditional generation in Appendix [A.6](#)
7. Limitations of GLASS in Appendix [A.7](#)

### A.1 Training details

GLASS for the COCO dataset is trained using an NVIDIA A100 GPU, and for the VOC dataset, we used an NVIDIA A6000 GPU. The training time for COCO models is typically 4–5 days, while for the VOC dataset, training is completed within two days. We used DINOv2 [51] model with ViT-B backbone using a patch size of 14 as the encoder model and a Stable Diffusion v2.1 [56] model as the decoder model. We repurposed the Stable Diffusion v2.1 [56] model to generate the guiding signal (semantic masks). We employed the standard slot attention module with 6 and 7 slots for the VOC and COCO datasets. The slot size is 768, and the number of GRU iterations for learning the slots is set to 3. Table 5 shows additional details about the hyper-parameters and modules used in GLASS. We will release the code upon acceptance.

### A.2 Training details for object-level property prediction

We train a single-layer MLP model for label prediction over 4K and 10K images from the VOC and COCO training sets, respectively. We used 1K validation images for choosing the best-performing model on the validation set. We report the results on 1K and 5K images chosen randomly from the VOC and COCO test sets. The models are trained for 6K steps, and the labels and slots are matched using the mask IoU criterion between the predicted masks from the slots and the ground-truth instance masks for real images. Since the VOC training dataset does not have instance masks, we compute the IoU criterion using the semantic mask.

Table 5: **Training details for GLASS.** Overview of the training details for GLASS on the COCO and VOC dataset.

Module	Hyperparameter	Dataset	
		VOC	COCO
General	Batch size	32	32
	Training steps	250K	500K
	Precision	fp16	fp16
	Learning rate	2e-5	2e-5
	Optimizer	Adam	Adam
	Learning rate scheduler	Constant	Constant
Encoder	Architecture	DINOv2	DINOv2
	Patch size	14	14
	Backbone	ViT-B	ViT-B
	Embedding dimension	768	768
Decoder	Arch	Stable Diffusion	Stable Diffusion
	Model number	2.1	2.1
SlotAttention	Slots	6	7
	Iteration	3	3
	Slot dimension	768	768

Table 6: **Comparison with other guiding signals.** We compare GLASS to other guidance signals used for weakly supervising the StableLSD model. StableLSD-BBox init uses bounding box information for initializing the slots. StableLSD-Mask and StableLSD-Box use ground truth semantic masks and ground truth bounding boxes for guiding the slots. GLASS, which uses low-cost guidance in the form of captions, achieves only slightly lower or even stronger performance compared to the more expensive guiding signals. The best value is highlighted in **red**, the second best in **blue**.

Model	Cost of annotation	COCO			VOC		
		mBO <sub>i</sub>	mBO <sub>c</sub>	mIoU	mBO <sub>i</sub>	mBO <sub>c</sub>	mIoU
StableLSD	None	25.85	30.04	29.55	30.41	43.08	32.95
StableLSD-Mask	Very High	<a href="#">38.69</a>	<b>51.54</b>	<b>48.68</b>	56.06	63.17	61.72
StableLSD-Box	High	<b>39.21</b>	<a href="#">46.88</a>	<a href="#">45.33</a>	46.29	50.99	48.64
StableLSD-Bbox Init	High	22.81	30.34	24.92	43.40	38.22	36.72
GLASS <sup>†</sup> (ours)	Low	34.35	45.23	42.38	<b>60.44</b>	<b>68.40</b>	<b>67.82</b>
GLASS (ours)	Low	35.27	46.28	43.72	<a href="#">58.07</a>	<a href="#">65.47</a>	<a href="#">64.00</a>

### A.3 Comparison with other guiding signals

We now aim to answer the question: *How does our generated pseudo-mask compare to stronger forms of guidance signal, such as ground-truth semantic masks and bounding boxes, and does using the guidance signal in another way, for example, using a bounding box for informed slot initialization instead of random initialization, work better than our proposed way of using the guidance information?*

For the COCO dataset bounding box as a guidance signal performs the best, followed by ground truth semantic masks (see Table 6). GLASS and GLASS<sup>†</sup> are still comparable to these methods when considering the time and cost required to obtain these guiding signals, indicating that our pseudo-ground truth semantic mask is not so far from the ground truth semantic mask. The cost of annotating semantic masks is very high as it requires pixel-wise labels. Similarly, bounding box annotation also requires a high amount of human labeling. Whereas GLASS and GLASS<sup>†</sup> use generated captions from BLIP-2, which is trained on image and caption pairs from the internet, which are ubiquitous on the web and thus require minimal human labeling effort. Interestingly, we find that GLASS and GLASS<sup>†</sup> using just generated captions outperform all other forms of guidance signals on the VOC dataset. We attribute it to the training images for GLASS and GLASS<sup>†</sup> being in distribution with the decoder model and to VOC being a comparatively simple dataset with many images containing only a single object. We observed that the generated semantic masks from the diffusion models are as good as the ground truth semantic masks for images with a single object.

We also see that the performance depends on how the ground truth signal is used. Using the bounding box information for slot initialization as proposed in [40] (StableLSD-Bbox Init) is inferior to StableLSD-Box on all metrics, *i.e.* using bounding box information as proposed in our architecture with our *guidance loss* outperforms using bounding box information for initializing the slots.

### A.4 General purpose guidance signal

Our proposed use of guidance signal is not tied to any particular encoder and decoder architecture. The semantic mask can be generated using a pre-trained diffusion model, and it can be used as a guidance signal with any slot attention architecture, *i.e.* our guidance method can also be used with other encoder and decoder architectures employed in any slot attention-based method. To verify this, we applied our guidance method to the DINOSAUR model for the object discovery task. The method for semantic mask generation and guidance is akin to Section 4, the only change compared to GLASS being that the DINOSAUR model uses a pre-trained DINO [8] model as its encoder and an MLP or transformer model [70] as its decoder. We propose two variants of DINOSAUR (*i*) DINOSAUR-Label that uses our guidance method with ground-truth class labels for guiding the slots and (*ii*) DINOSAUR-Caption that uses our guidance method with generated captions for guiding the slots. Both these variants use a DINO encoder model and an MLP decoder model. Table 7 shows that our proposed guidance framework helps slots to bind to objects, which results in performance improvement on key object discovery metrics such as mBO<sub>i</sub>, mBO<sub>c</sub>, and mIoU. The improvements for the COCO dataset range from approx. 5-11% on all the metrics, and for the VOC dataset, the

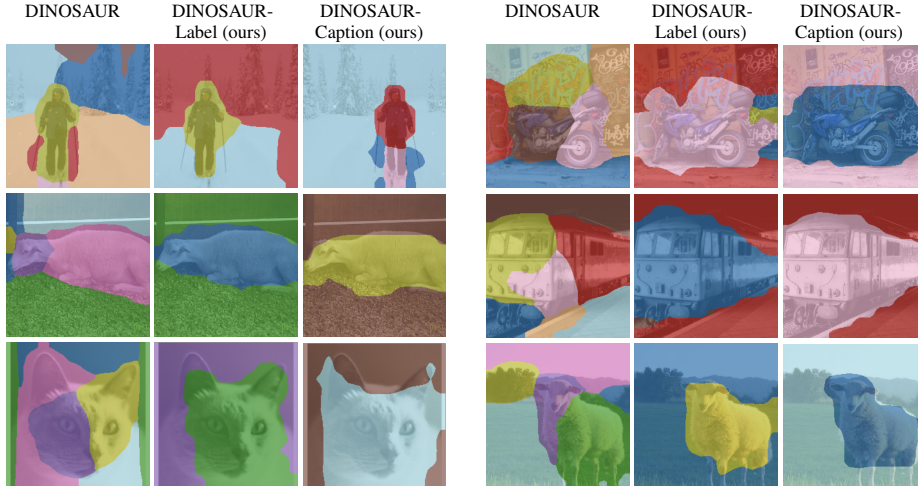


Figure 5: **Qualitative results when using our guidance generator module with DINO-SATUR model [63].** Our method is generic enough to be used with any decoder and encoder architecture employed in a slot-attention-based method. Here, we apply our method to a SOTA OCL method, DINO-SATUR. Our guidance signal helps DINO-SATUR to decompose scenes with no object splitting and cleaner segmentation for the background.

Table 7: **General purpose guidance.** Comparison between the vanilla DINO-SATUR and DINO-SATUR models with our guidance generator module. DINO-SATUR-Label uses ground truth class labels for guidance, while DINO-SATUR-Caption uses captions generated with the BLIP-2 model for guidance.

Model	COCO			VOC		
	mBO <sub>i</sub>	mBO <sub>c</sub>	mIoU	mBO <sub>i</sub>	mBO <sub>c</sub>	mIoU
DINO-SATUR-MLP	28.07	32.14	32.14	39.72	41.18	41.02
DINO-SATUR-Label (ours)	<b>30.92</b>	<b>39.34</b>	<b>37.96</b>	<b>46.20</b>	<b>51.96</b>	<b>50.35</b>
DINO-SATUR-Caption (ours)	<u>29.62</u>	<u>38.54</u>	<u>35.96</u>	<b>49.38</b>	<b>55.38</b>	<b>53.82</b>

improvements range from approx. 24-35% on all metrics. Fig. 5 shows qualitative results where it can be seen that our guidance helps achieve less object splitting, better background segmentation, and crisper boundaries for objects compared to the DINO-SATUR model [63].

### A.5 Additional qualitative results for object discovery task

Fig. 6 shows additional qualitative results for object discovery. GLASS decomposes the scene more cleanly and meaningfully when compared with SOTA OCL methods such as DINO-SATUR and StableLSD models. GLASS segmented images have more precise boundaries, background segmentation is much cleaner, and segmentation does not split the objects.

### A.6 Additional conditional generation results

Fig. 7 show additional results for the conditional generation of images using StableLSD, GLASS<sup>†</sup>, and GLASS. Our method generates images with higher fidelity than the StableLSD. This can be observed for various subjects ranging from animals, cars/buses, and food to human beings, *etc.* The reason for more realistic-looking image generation can be seen in how the methods decompose the objects. While GLASS and GLASS<sup>†</sup> bind slots to objects and capture their properties, StableLSD binds slots to object parts, leading to poor conditional generation. Please note that the generator module is frozen for all models, indicating the performance differences come from the learned slot embeddings only.

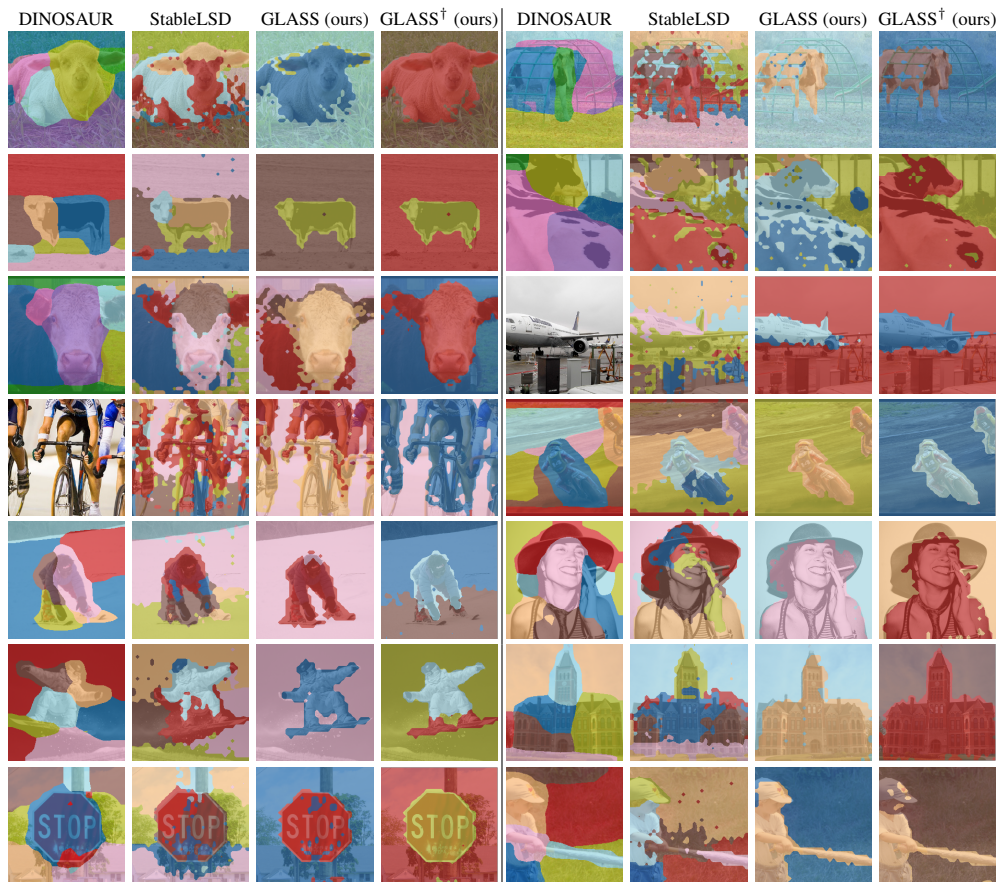


Figure 6: **Qualitative comparison for object discovery.** GLASS and GLASS<sup>†</sup> are able to decompose an image at an object level and do not decompose an object into subparts compared to SOTA OCL methods like DINOSAUR and StableLSD. They segment objects with crisper boundaries and cleaner background segmentation compared to StableLSD and DINOSAUR.

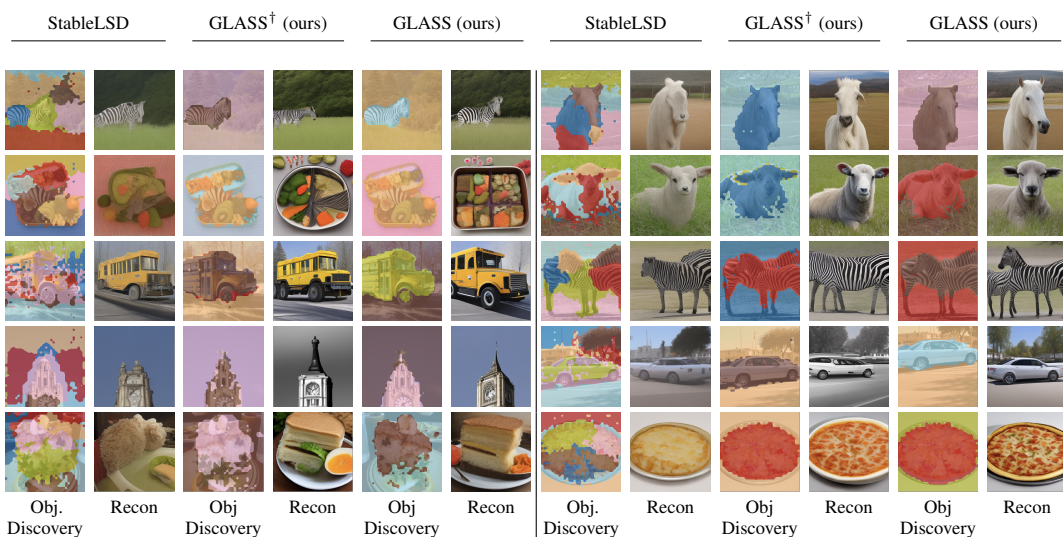


Figure 7: **Qualitative comparison for conditional image generation.** GLASS and GLASS<sup>†</sup> not only learn to decompose scenes meaningfully, but this decomposition also leads to higher fidelity conditional image generation.



Figure 8: **Drawbacks.** Our guided slot attention model binds slots to semantic classes instead of instances. This causes it to group object classes together; this issue was also observed when using a transformer decoder with the DINOSAUR model [63].

### A.7 Limitations

GLASS uses generated images and their corresponding pseudo ground-truth masks to guide the slot attention module. However, the generated masks are semantic and not instance masks. This causes GLASS to bind slots to semantic classes instead of instances (Fig. 8). A possible solution to resolve the issue could be using zero-shot methods like [44] for generating bounding boxes instead of masks and using them as guiding signals.